Disentangling Electronic and Ionic Nonlinear Polarization Effects in Bulk THz Kerr Response

Chao Shen,[1] Maximilian Frenzel,[2] Sebastian F. Maehrlein,[2,3,4] and Zhanybek Alpichshev[1,*]
[1]ISTA (Institute of Science and Technology Austria), Klosterneuburg 3400, Austria
[2]Fritz Haber Institute of the Max Planck Society, Department of Physical Chemistry, Berlin, Germany
[3]Helmholtz-Zentrum Dresden-Rossendorf, Institute of Radiation Physics, Dresden, Germany
[4]Dresden University of Technology, Institute of Applied Physics, Dresden, Germany

(Received 12 June 2025; accepted 3 February 2026; published 9 March 2026)

Terahertz (THz) spectroscopy is a powerful probe of low-energy excitations in complex materials. Extending it into the nonlinear regime broadens its scope and can provide valuable insight into interactions among these modes. However, interpreting nonlinear spectra is challenging because resonant features in this case do not always reflect intrinsic material dynamics. Here, we study nonlinear THz-induced Kerr effect in a generic material $LaAlO_3$. After detailed analysis of temporal oscillations of the Kerr signal, we identify an E_g Raman mode at 1.1 THz excited through a two-photon process, while two additional peaks (0.86 and 0.36 THz) arise from phase matching of the near-infrared probe beam with co- and counterpropagating THz pump fields, mediated by off-resonant electronic hyperpolarizability. These results demonstrate the crucial role of kinematic effects in shaping THz-induced Kerr response and establish a framework for interpreting nonlinear spectroscopies in complex materials.

DOI: 10.1103/1c5k-9z82

The advent of tabletop sources of intense terahertz (THz) pulses has made it possible to directly explore low-energy modes while keeping electronic degrees of freedom largely unaffected [1–5]. In high-field THz spectroscopies, intense THz pulses are used to excite low-lying degrees of freedom (e.g., phonons, magnons, etc.) that can undergo nonlinear mutual interactions. The resulting real-time dynamics can be obtained by sensing the modified response of the host medium. One method developed recently is two-dimensional THz Kerr effect spectroscopy (2D-TKE), whereby two THz pulses are used to excite infrared- and Raman-active modes, which modify refractive index of the medium through Kerr effect picked up by a near-infrared probe beam [6–10]. Distinct excitation pathways of Raman-active phonons appear as characteristic patterns in the time- and frequency-domain responses, enabling direct comparison of experimental data with theoretical models [6]. However, great care must be taken when interpreting such data. Unlike in linear spectroscopy, where every spectral feature corresponds to a resonance mediated by an actual dynamical mode of the material, nonlinear spectroscopic techniques—such as TKE—involve complex interactions between multiple waves. In such cases, one can no longer assume that every instance of resonant enhancement in a nonlinear process necessarily reflects a dynamical mode of the host material. In particular, in the case of extended samples, well-defined spectral peaks can emerge on purely kinematic grounds (e.g., phase matching between pump and probe) that do not correspond to any dynamical modes of the material [11,12].

$LaAlO_3$ (LAO) is a common wide-gap insulator ($\Delta \approx 5.5$ eV) widely used as a substrate for the epitaxial growth of quantum materials. Recent single pulse TKE measurements show complex temporal oscillations at both room and low temperatures that could not be entirely accounted for using Raman spectra of LAO reported in the literature [14,15]. The main complication in the analysis of TKE data comes from the fact that below $T \approx 813$ K LAO is characterized by the rhombohedral (D_{3d} point group) lattice structure implying that it is birefringent for both THz and optical probe pulses. This will unavoidably give rise to rich and complex interaction dynamics between THz and near-infrared probe pulses, including non-negligible propagation effects in THz Kerr response.

In this Letter, we report 2D-TKE measurements on LAO supported by detailed theoretical modeling based on four-wave mixing (FWM) simulation in an extended medium to unravel the complex third-order nonlinear THz polarization in bulk LAO samples at cryogenic temperatures. Similar to previous reports [15], we observe three distinct frequencies in TKE response (1.1, 0.86, and 0.36 THz). Using time-domain 2D-TKE spectroscopy we show that while

*Contact author: alpishev@ist.ac.at

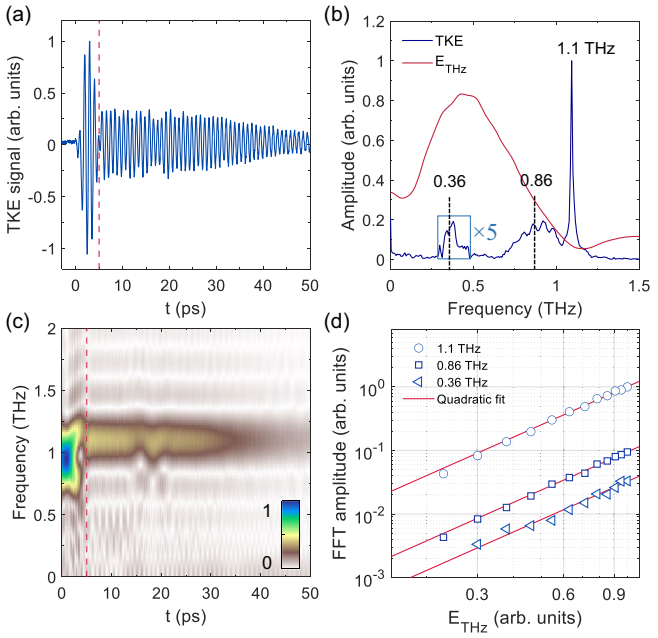

FIG. 1. Single pulse TKE measurement and field scaling of LAO at $T = 5$ K. (a) Representative single pulse TKE signal at $T = 5$ K. The red dashed line at 5 ps indicates the delay when THz and 800 nm probe pulses meet at the rear surface of LAO. (b) Spectra of THz pulse and fast Fourier transform (FFT) of (a). (c) Normalized short-time FFT of (a) with a 4 ps Kaiser window. The dashed line is the same as (a). (d) Field scaling of peaks at 1.1, 0.86, and 0.36 THz.

$f = 1.1$ THz mode shows typical features of the coherent E_g Raman phonon in agreement with literature, the novel features at 0.86 and 0.36 THz only occur within specific delay ranges, indicative of propagation effect. In addition, 2D-TKE provides clear evidence that the excitation channel of E_g phonon corresponds to two-photon THz absorption, while the reflection of THz pulses at the sample surface can mimic anharmonic phonon coupling. Our FWM simulations that account for the birefringence of both THz pump- and near-infrared probe pulses quantitatively reproduce all of the novel features, unambiguously distinguishing instantaneous electronic polarization from the genuine Raman response of the material.

We excite a [100]-cut 0.5 mm-thick LAO with an intense single-cycle THz pump pulse (peak field $E_p \approx 640$ kV/cm) generated by means of optical rectification of 170 fs-long 800 nm pulses in $LiNbO_3$ [16,17] and the transient Kerr effect-induced birefringence is probed by an additional 800 nm pulse arriving at a controllable delay t relative to the pump.

Figure 1(a) shows the TKE signal at $T = 5$ K. The data exhibit pronounced oscillations that start immediately at the arrival of the THz pulse. Figure 1(b) shows the Fourier amplitude of single pulse TKE signal together with the THz excitation spectrum. Three peaks are visible here: a sharp and strong mode at 1.1 THz, a broad hump-like mode around 0.86 THz, and a much weaker peak at 0.36 THz. The feature at 1.1 THz has been reported previously and was consistently identified as the E_g Raman mode of LAO. We confirm this attribution by observing the intensity of the peak scaling quadratically as a function of incident THz field strength [Fig. 1(d), top line]. The central frequency and amplitude of the E_g mode exhibit slight dependence on the lateral sample position. Since the mode frequency is associated with rotations of the AlO_6 octahedra about the [111] direction, this variation can be attributed to local structural variations accompanying the transition from the cubic to the rhombohedral phase [18]. In contrast with the 1.1 THz peak, the features at 0.86 and 0.36 THz do not correspond to any known lattice modes of the rhombohedral lattice of LAO. To clarify the origin of these peaks, we proceed to investigate the time dependence of TKE signal in Fig. 1(a): we perform a short-time Fourier transform with a 4 ps-wide moving window [Fig. 1(c)] and observe that unlike 1.1 THz peak, which exists for all time positions of the Fourier window, the 0.86 THz feature is only there for probe delay times less than some characteristic cutoff time $\tilde{t} \approx 5$ ps. Referring back to Fig. 1(a) we notice that $\tilde{t}$ is even more prominent in time domain, marking a visible change in the TKE signal. Using previously reported values for cryogenic refractive indices $n_{\mathrm{THz}} = 5$ between 0.4 and 1 THz [15] and $n_{\mathrm{pr}} \approx 2$ at 800 nm [19], we find that $\tilde{t}$ corresponds exactly to the moment when THz pump and near-infrared probe pulses meet at the rear surface of the sample, hinting that at least the 0.86 THz feature arises from propagation effects. This is further supported by the presence of multiple equidistant peaks on top of the 0.86 THz feature with a spacing of 0.06 THz, which can be explained by THz Fabry-Perot modes existing in a 0.5 mm-thick sample [20]. In agreement with centrosymmetric symmetry of LAO that dictates that all features visible in Kerr effect result from a third-order nonlinear polarization [21], the intensities of both 0.36 and 0.86 THz features scale quadratically as a function of THz field strength [Fig. 1(d)].

More information on the nature of the observed peaks can be revealed by two-dimensional spectroscopy. To this end, two individual THz pulses with a controllable delay τ are produced in separate $LiNbO_3$ crystals. The pump delay τ is introduced such that one of pump pulses is fixed in time (THz A) while the other one is time-delayed relative to it (THz B). A weak near-infrared pulse at 800 nm wavelength for probing comes with a probe delay t relative to THz A. We performed 2D-TKE measurements on LAO at $T = 5$ K with both THz pump pulses polarized at 45° with respect to the c axis of the crystal and probe polarization was aligned parallel to the c axis. The measured quantity is the so-called nonlinear ellipticity η_{NL} defined as $\eta_{\mathrm{NL}} \equiv \eta_{\mathrm{AB}} - \eta_{\mathrm{A}} - \eta_{\mathrm{B}}$, where η_{A}, η_{B}, and η_{AB} stand for the Kerr signal induced by THz A alone, THz B alone, and both pulses together,

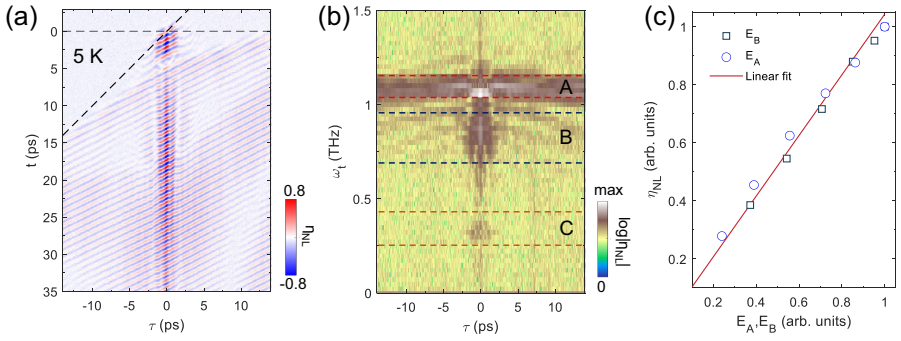

FIG. 2. Nonlinear 2D-TKE measurements of LAO at $T = 5$ K. (a) Normalized temporal signal of nonlinear 2D-TKE. The dashed lines indicate the causality lines, namely the moment when the THz pulse arrives at the sample. (b) FFT of (a) along the t axis. (c) Field scaling of nonlinear signal η_{NL} at 1.1 THz as a function of E_{A} and E_{B}, respectively. The signal is sampled along the $\tau = 0$ line. In each measurement, the field of the other THz pulse was set to maximum.

respectively [22]. The details of the experiment can be found in Supplemental Material [12] and Ref. [23].

The nonlinear 2D-TKE signal η_{NL} is shown in Fig. 2(a). Here, t corresponds to the delay of probe pulse relative to THz A, while τ is the timing between two THz pump pulses. The 2D-TKE technique makes it possible to see how signal in Fig. 1 depends on the delay between two THz pulses, in particular, the spectral content of it, as shown in Fig. 2(b). We first note that the 1.1 THz Raman mode is excited most efficiently when both THz pulses overlap in time ($\tau \approx 0$), strongly suggesting the E_g phonon is primarily excited through direct instantaneous two-photon THz absorption. We further confirm this by observing that the magnitude of the main 1.1 THz peak at $\tau = 0$ scales linearly with field intensities of both THz pulses [Fig. 2(c)]. On the other hand, however, it is easy to notice that 1.1 THz oscillations also persist at $\tau \neq 0$—albeit with reduced magnitude—which could be indicative of an anharmonic coupling between IR-active and Raman-active phonons that would appear as extended features in τ direction. However, a closer inspection of the data in Fig. 2(a) reveals that for $\tau \neq 0$ the 1.1 THz oscillations do not begin right after the arrival of the latest THz pulse, but instead start off with a visible delay in probe time t, which suggests propagation phenomena behind $\tau \neq 0$ oscillations as well.

To clarify the mechanism behind 1.1 THz excitation as well as the physical nature of 0.36 and 0.86 THz peaks we trace the probe-time dependence of each of the peaks in Fig. 2(b) by performing inverse Fourier transform (IFFT) of each of the segments in probe-frequency ω_t domain separately. Figures 3(a)–3(c) show the inverse transforms of regions A, B, and C in Fig. 2(b), respectively. Figure 3(a) shows that the 1.1 THz oscillations at $\tau \neq 0$ begin at what we refer to as the "echo line" [see lower panel in Fig. 3(d)], which for every given value of pump delay τ corresponds to probe time t at which one of the THz pulses meets with the other THz pulse that was backreflected from the rear surface of the sample [23],

$$t + \frac{\tau}{2}\left(1 - \mathrm{sgn}(\tau)\frac{v}{c}\right) = L\left(\frac{1}{v} - \frac{1}{c}\right), \tag{1}$$

where L is the thickness of the sample. This suggests an intuitive interpretation for the 1.1 THz oscillations at $\tau \neq 0$ as E_g Raman mode quasi-instantaneously excited by two counterpropagating THz pulses.

Turning to the 0.86 and 0.36 THz features in Figs. 3(b) and 3(c), respectively, we observe a behavior inconsistent with coherent phonon oscillations. A coherent phonon cannot switch on or off at geometrically defined times, yet the 0.86 THz oscillation begins at $t = 0$ ps and terminates sharply at $\tilde{t} \approx 5$ ps, when the probe and both pump pulses meet at the rear surface of the sample ($\tau = 0$) [upper panel of Fig. 3(d)]. Conversely, the 0.36 THz oscillation [Fig. 3(c)] appears abruptly at $\tilde{t}$ and vanishes at $\tilde{t}_2 \approx 17$ ps, when the probe pulse meets the backreflected pump pulses at the front surface ($\tau = 0$) [upper panel of Fig. 3(d)]. Such behavior rules out phononic or any other intrinsic dynamical mechanism behind these spectral features and instead points to propagation effects. It can be shown that in Kerr effect in a bulk sample, the kinematic constraints of energy and momentum conservation (phase matching) can favor specific energy transfer between pump and probe photons, yielding characteristic frequency $\Omega_{\mathrm{kin}} = \omega_{\mathrm{pr}}^{\mathrm{out}} - \omega_{\mathrm{pr}}^{\mathrm{in}}$ set by refractive index dispersion and by the geometry of the nonlinear interaction [12,24]. This "kinematic resonance" manifests itself as Kerr signal oscillations at Ω_{kin}, providing a natural explanation for both the 0.86 and 0.36 THz features and their distinctive dependence on the mutual orientation of pump and probe propagation directions.

For quantitative analysis we utilize a FWM simulation based on the THz-THz-VIS scheme that was recently introduced to analyze the TKE in bulk samples [11] (see End Matter). The simulated 2D-TKE, shown in Figs. 3(f) and 3(g), features pronounced short-lived oscillations of 0.85 THz that end abruptly at around $t = 5$ ps [Fig. 3(f)], when slower short-lived oscillations of 0.39 THz appear,

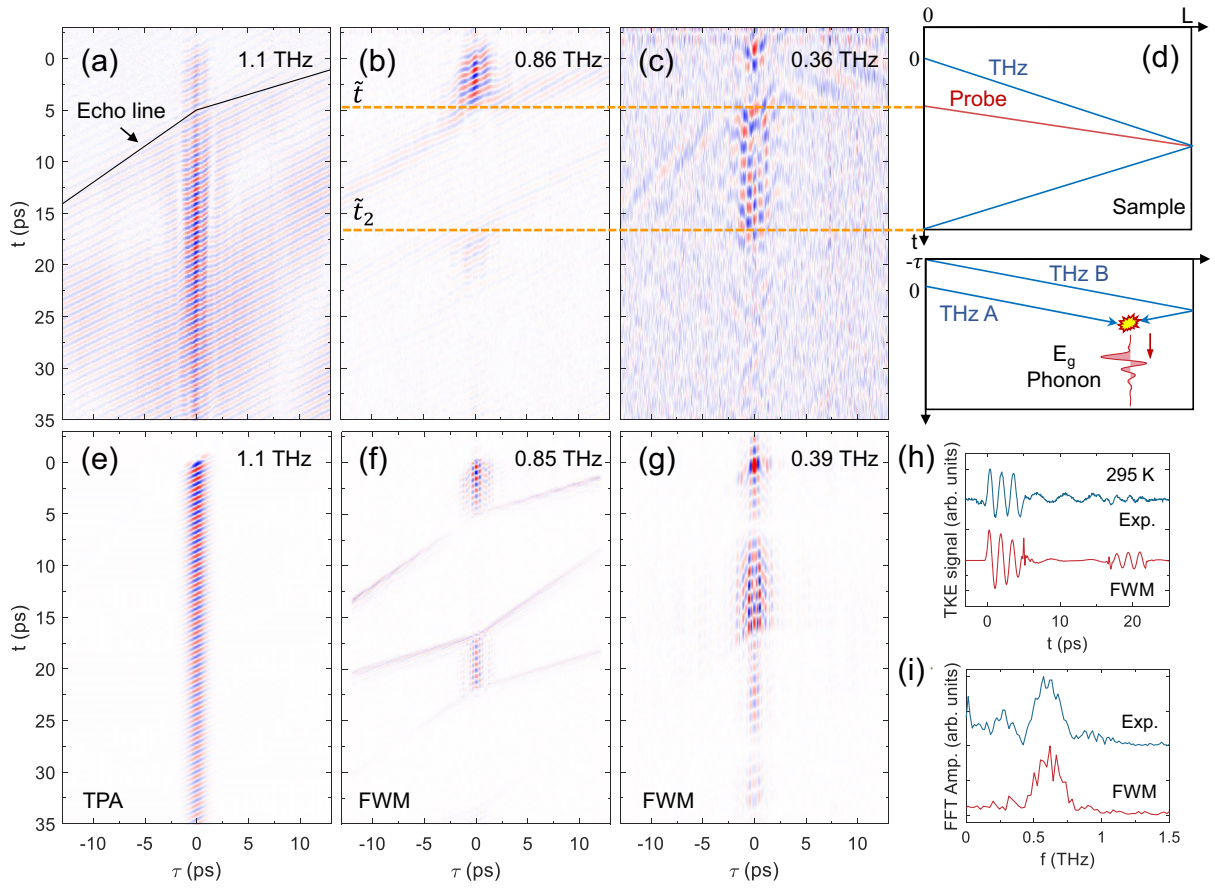

FIG. 3. IFFT of three peaks and modeling. (a)–(c) IFFT of the 1.1, 0.86, and 0.36 THz peaks, respectively. (d) Upper panel: world line diagram at $\tau = 0$, illustrating the propagation and reflection of the THz and optical probe pulses within the sample. Lower panel: world line diagram for $\tau > 0$. The explosion symbol marks the point where two THz pulses intersect. The collection of these points at varying τ defines the echo line shown in panel (a). (e) Simulation of 1.1 THz mode using TPA. (f),(g) FWM simulation of 0.86 and 0.36 THz peaks, respectively. (h) Measured and FWM simulated single pulse TKE response at room temperature. (i) FFT of panel (h).

which stop at $t = 16.8$ ps [Fig. 3(g)]. Similar agreement can be also found in the single pulse TKE measurement at room temperature, as shown in Figs. 3(h) and 3(i). The simulation results thus agree with the experimental measurements, and confirm the attribution of the 0.86 and 0.36 THz signals in the 2D-TKE to the kinematic enhancement of Kerr interaction between THz pump and near-infrared probe. This conclusion is further substantiated by similar measurements performed on a 1 mm-thick sample, confirming that all three frequencies do not depend on sample thickness [12].

Finally, we discuss the excitation pathway of E_g phonon. Because of the lack of dipole moment, Raman-active phonons in centrosymmetric media can only be excited through an indirect process [25], such as anharmonic coupling to IR-active phonons, two-photon absorption (TPA) [26], or the recently proposed hybrid photon-phonon excitation [27]. As discussed above, the experiment points toward TPA as the excitation mechanism. This is further corroborated by the fact that there is no known IR-active phonon within the bandwidth of the THz pump pulses [Fig. 1(b)] [28]. To elaborate on this assumption, we simulate the temporal evolution of the E_g phonon coordinate $Q_{\mathrm{R}}(t)$ by solving the harmonic-oscillator-type equation of motion driven by the force term proportional to $E^2_{\mathrm{THz}}(t)$ (see Supplemental Material [12]). The nonlinear signal is calculated using $Q_{\mathrm{R_{NL}}} \propto Q_{\mathrm{R_{AB}}} - Q_{\mathrm{R_A}} - Q_{\mathrm{R_B}}$, where $Q_{\mathrm{R_A}}$, $Q_{\mathrm{R_B}}$, and $Q_{\mathrm{R_{AB}}}$ stand for the E_g phonon coordinate excited by THz A or THz B pulses alone, or with both together, respectively. As shown in Fig. 3(e), simulated $Q_{\mathrm{R_{NL}}}$ agrees well with experimental 2D-TKE signal from E_g phonon, save for the contribution from backreflection of THz pulses, not included in this calculation. Note that this process is not phase matched and thus nominally forbidden in extended media. It occurs only when the momentum conservation requirement is relaxed: near the sample surface or when two THz pulses collide within the bulk, justifying the local oscillator description [12].

In summary, we have investigated the THz Kerr response in a bulk material using 2D THz Kerr effect spectroscopy. Our analysis shows that, in addition to the conventional

phonon-mediated resonances, prominent peaks in the TKE spectrum can also originate from phase matching between the THz and probe beams, which do not correspond to any dynamical modes within the material. These features therefore represent "kinematic" rather than "dynamical" resonances of the nonlinear TKE process. Our results refine the interpretation of nonlinear THz responses across a broad class of dielectrics, including $LaAlO_3$, $SrTiO_3$ [23], and $KTaO_3$ [29], where THz fields propagate as light pulses or phonon-polaritons, and provide a foundation for reliably identifying genuine dynamical lattice phenomena in future studies of ultrafast light-matter interactions.

Acknowledgments—Z. A. acknowledges support from the collaborative research project SFB Q-M&S funded by the Austrian Science Fund (FWF, Grant No. PR1050F8602). S. F. M. acknowledges support and funding from the Deutsche Forschungsgemeinschaft (DFG, Grant No. 469405347).

Data availability—The data that support the findings of this article are not publicly available because of legal restrictions preventing unrestricted public distribution. The data are available from the authors upon reasonable request.

[1] M. Liu, H. Y. Hwang, H. Tao, A. C. Strikwerda, K. Fan, G. R. Keiser, A. J. Sternbach, K. G. West, S. Kittiwatanakul, J. Lu *et al.*, Terahertz-field-induced insulator-to-metal transition in vanadium dioxide metamaterial, Nature (London) **487**, 345 (2012).

[2] X. Li, T. Qiu, J. Zhang, E. Baldini, J. Lu, A. M. Rappe, and K. A. Nelson, Terahertz field–induced ferroelectricity in quantum paraelectric $SrTiO_3$, Science **364**, 1079 (2019).

[3] S. Pal, N. Strkalj, C.-J. Yang, M. C. Weber, M. Trassin, M. Woerner, and M. Fiebig, Origin of terahertz soft-mode nonlinearities in ferroelectric perovskites, Phys. Rev. X **11**, 021023 (2021).

[4] B. Song, X. Yang, C. Sundahl, J.-H. Kang, M. Mootz, Y. Yao, I. Perakis, L. Luo, C. Eom, and J. Wang, Ultrafast martensitic phase transition driven by intense terahertz pulses, Ultrafast Science **3**, 0007 (2023).

[5] M. Basini, M. Pancaldi, B. Wehinger, M. Udina, V. Unikandanunni, T. Tadano, M. Hoffmann, A. Balatsky, and S. Bonetti, Terahertz electric-field-driven dynamical multiferroicity in $SrTiO_3$, Nature (London) **628**, 534 (2024).

[6] C. L. Johnson, B. E. Knighton, and J. A. Johnson, Distinguishing nonlinear terahertz excitation pathways with two-dimensional spectroscopy, Phys. Rev. Lett. **122**, 073901 (2019).

[7] H.-W. Lin, G. Mead, and G. A. Blake, Mapping $LiNbO_3$ phonon-polariton nonlinearities with 2D THz-THz-Raman spectroscopy, Phys. Rev. Lett. **129**, 207401 (2022).

[8] T. G. H. Blank, K. A. Grishunin, K. A. Zvezdin, N. T. Hai, J. C. Wu, S.-H. Su, J.-C. A. Huang, A. K. Zvezdin, and A. V. Kimel, Two-dimensional terahertz spectroscopy of nonlinear phononics in the topological insulator $MnBi_2Te_4$, Phys. Rev. Lett. **131**, 026902 (2023).

[9] Z. Zhang, J. Zhang, Z.-J. Liu, N. S. Dahod, W. Paritmongkol, N. Brown, A. Stollmann, W. S. Lee, Y.-C. Chien, Z. Dai, K. A. Nelson, W. A. Tisdale, A. M. Rappe, and E. Baldini, Discovery of enhanced lattice dynamics in a single-layered hybrid perovskite, Sci. Adv. **9**, eadg4417 (2023).

[10] O. Minakova, C. Paiva, M. Frenzel, M. S. Spencer, J. M. Urban, C. Ringkamp, M. Wolf, G. Mussler, D. M. Juraschek, and S. F. Maehrlein, Direct observation of angular momentum transfer among crystal lattice modes, arXiv:2503.11626.

[11] M. Frenzel, M. Cherasse, J. M. Urban, F. Wang, B. Xiang, L. Nest, L. Huber, L. Perfetti, M. Wolf, T. Kampfrath *et al.*, Nonlinear terahertz control of the lead halide perovskite lattice, Sci. Adv. **9**, eadg3856 (2023).

[12] See Supplemental Material at http://link.aps.org/supplemental/10.1103/1c5k-9z82 for (1) the experimental setup, (2) details of sample, (3) simulation details of four-wave mixing of the 2D-TKE signal, (4) analytical treatment of THz Kerr effect, and (5) simulation details of E_g Raman phonon, which includes Ref. [13].

[13] S. F. Maehrlein, P. P. Joshi, L. Huber, F. Wang, M. Cherasse, Y. Liu, D. M. Juraschek, E. Mosconi, D. Meggiolaro, F. De Angelis *et al.*, Decoding ultrafast polarization responses in lead halide perovskites by the two-dimensional optical Kerr effect, Proc. Natl. Acad. Sci. U.S.A. **118**, e2022268118 (2021).

[14] S. Kovalev, C. Zhu, A. Reinold, M. Koch, Z. Wang, P. Pilch, A. Ghalgaoui, S. Duan, C. Li, J. Zhang *et al.*, Terahertz electro-optic Kerr effect in $LaAlO_3$, Opt. Lett. **50**, 762 (2025).

[15] M. Basini, V. Unikandanunni, F. Gabriele, M. Cross, A. Derrico, A. Gray, M. Hoffmann, F. Forte, M. Cuoco, and S. Bonetti, Terahertz-driven parametric excitation of Raman-active phonons in $LaAlO_3$, arXiv:2410.06748.

[16] J. Hebling, G. Almasi, I. Z. Kozma, and J. Kuhl, Velocity matching by pulse front tilting for large-area THz-pulse generation, Opt. Express **10**, 1161 (2002).

[17] H. Hirori, A. Doi, F. Blanchard, and K. Tanaka, Single-cycle terahertz pulses with amplitudes exceeding 1 MV/cm generated by optical rectification in $LiNbO_3$, Appl. Phys. Lett. **98**, 091106 (2011).

[18] E. K. Salje, M. Alexe, S. Kustov, M. C. Weber, J. Schiemer, G. F. Nataf, and J. Kreisel, Direct observation of polar tweed in $LaAlO_3$, Sci. Rep. **6**, 27193 (2016).

[19] C. M. Nelson, M. Spies, L. S. Abdallah, S. Zollner, Y. Xu, and H. Luo, Dielectric function of $LaAlO_3$ from 0.8 to 6 eV between 77 and 700 K, J. Vac. Sci. Technol. A **30**, 061404 (2012).

[20] M. S. Spencer, J. M. Urban, M. Frenzel, N. S. Mueller, O. Minakova, M. Wolf, A. Paarmann, and S. F. Maehrlein, Electro-optic cavities for in-situ measurement of cavity fields, Light **14**, 69 (2025).

[21] J. M. Urban, M. S. Spencer, M. Frenzel, G. Trippé-Allard, M. Cherasse, C. Berrezueta-Palacios, P. P. Joshi, A. P. Fellows, O. Minakova, E. B. Barros, L. Perfetti, S. Reich, M. Wolf, E. Deleporte, and S. F. Maehrlein, THz-driven coherent phonon fingerprints of hidden symmetry breaking in 2D layered hybrid perovskites, Adv. Mater. **38**, e02204 (2026).

[22] J. Lu, X. Li, H. Y. Hwang, B. K. Ofori-Okai, T. Kurihara, T. Suemoto, and K. A. Nelson, Coherent two-dimensional terahertz magnetic resonance spectroscopy of collective spin waves, Phys. Rev. Lett. **118**, 207204 (2017).
[23] C. Shen, C. Verdi, S. Babkin, M. Serbyn, and Z. Alpichshev, Nonlinear terahertz polaritonics in a quantum paraelectric, arXiv:2507.19358.
[24] L. Huber, S. F. Maehrlein, F. Wang, Y. Liu, and X.-Y. Zhu, The ultrafast Kerr effect in anisotropic and dispersive media, J. Chem. Phys. **154**, 094202 (2021).
[25] D. M. Juraschek and S. F. Maehrlein, Sum-frequency ionic Raman scattering, Phys. Rev. B **97**, 174302 (2018).
[26] S. Maehrlein, A. Paarmann, M. Wolf, and T. Kampfrath, Terahertz sum-frequency excitation of a Raman-active phonon, Phys. Rev. Lett. **119**, 127402 (2017).
[27] G. Khalsa, N. A. Benedek, and J. Moses, Ultrafast control of material optical properties via the infrared resonant Raman effect, Phys. Rev. X **11**, 021067 (2021).
[28] M. V. Abrashev, A. P. Litvinchuk, M. N. Iliev, R. L. Meng, V. N. Popov, V. G. Ivanov, R. A. Chakalov, and C. Thomsen, Comparative study of optical phonons in the rhombohedrally distorted perovskites $LaAlO_3$ and $LaMnO_3$, Phys. Rev. B **59**, 4146 (1999).
[29] X. Li, P. Peng, H. Dammak, G. Geneste, A. Akbarzadeh, S. Prosandeev, L. Bellaiche, and D. Talbayev, Terahertz pulse induced second harmonic generation and Kerr effect in the quantum paraelectric $KTaO_3$, Phys. Rev. B **107**, 064306 (2023).

End Matter

For TKE simulation, we model the third-order nonlinear polarization using the general expression

$$P_i^{(3)}(t,z) = \epsilon_0 \int_{-\infty}^{t} dt' \int_{-\infty}^{t'} dt'' \int_{-\infty}^{t''} dt''' \tilde{R}_{ijkl} \times R(t,t',t'',t''') E_j^{\mathrm{THz}}(t',z) \times E_k^{\mathrm{THz}}(t'',z) E_l^{\mathrm{pr}}(t''',z), \tag{A1}$$

where z corresponds to the spatial axis, along the direction of propagation of the THz (E^{THz}) and probe (E^{pr}) fields. Here, $R(t,t',t'',t''')$ is the time-domain $\chi^{(3)}$ response function analog, and $\tilde{R}_{ijkl}$ captures the crystal symmetry. To focus on the instantaneous electronic hyperpolarizability including static birefringence and pump-probe walk-off, we model a product of temporal Dirac delta functions, $R(t,t',t'',t''') = R_{\mathrm{e},0}\delta(t-t')\delta(t'-t'')\delta(t''-t''')$. To compute $P_i^{(3)}(t,z)$, all three contributing light fields, E_j^{THz}, E_k^{THz}, and E_l^{pr} are propagated through the crystal on a time-space grid [24]. The computed local $P_i^{(3)}(t,z)$ acts as a source for the emitted field $E_i^{(4)}(t,z)$ via the one-dimensional inhomogeneous wave equation. $E^{(4)}(t,z)$ ultimately interferes with the copropagating probe field E^{pr} in a balanced detection to give rise to the Kerr effect signal. In contrast to Ref. [11], we simulate a double THz pump scheme, with a variable temporal delay τ between two THz pulses. More details on the simulation can be found in Supplemental Material [12].